Type Paper Number Here

Modeling n-dodecane spray combustion with a representative interactive linear eddy model

Author, co-author (Do NOT enter this information. It will be pulled from participant tab in MyTechZone)

Affiliation (Do NOT enter this information. It will be pulled from participant tab in MyTechZone)

ABSTRACT

Many new combustion concepts are currently being investigated to further improve engines in terms of both efficiency and emissions. Examples include homogeneous charge compression ignition (HCCI), lean stratified premixed combustion, stratified charge compression ignition (SCCI), and high levels of exhaust gas recirculation (EGR) in diesel engines, known as low temperature combustion (LTC). Typical combustion temperatures in all of these combustion concepts have in common that the temperatures are lower than in traditional spark ignition or diesel engines.

To further improve and develop combustion concepts for clean and highly efficient engines, it is necessary to develop new computational tools that can be used to describe and optimize processes in non-standard conditions, such as low temperature combustion. Thus, in the presented study a recently developed model (RILEM: Representative Interactive Linear Eddy Model [1]) for a regime-independent modeling of turbulent non-premixed combustion is used to simulate the so called 'Spray B' of the Engine Combustion Network (ECN), which is a heavy-duty optical engine experiment. The RILEM directly resolves the interaction of turbulent mixing with the chemistry along a one-dimensional representative line of sight through the combustion chamber via a stochastic sequences of statically independent eddy events. The RILEM in the present form consists of a single (one-dimensional) linear eddy model (LEM) that is coupled to an unsteady Reynolds-averaged Navier-Stokes solver within the OpenFOAM framework. The coupling is similar to unsteady flamelet concepts but features distinct and important differences, e.g. an intrinsic representation of the scalar dissipation rate distribution and its fluctuations. Cylinder pressure, heat release rates and ignition delay time from the computation are compared to experiments under parametric variation of temperatures.

INTRODUCTION

Engine development aims at reducing pollutant emissions (NOx and soot) while maintaining high efficiencies. Detailed experimental results in combination with precise numerical predictions are of great importance in order to develop combustion systems for new clean and efficient internal combustion engines.

Computational fluid dynamics (CFD) tools must be able to deal with multi-mode (premixed, partially premixed and non-premixed) and multi-regime (kinetically controlled vs. turbulent mixing controlled) turbulent combustion under various conditions (low temperatures, high pressures, high EGR rates). Work on laboratory flames (CITE) clearly show the strong need to account for the impact of unresolved turbulent fluctuations of temperature and composition on chemical reaction rates in Reynold-averaged and large-eddy simulations of turbulent combustion. Combustion models that neglect this so called 'turbulence-chemistry interaction' (TCI) cannot predict fundamental physical phenomena like local or global extinction which may lead to unprecise predictions of essential quantities including heat release rates, temperatures and emissions. Nevertheless, a lot of internal combustion engine studies involving non-premixed combustion use stirred/partially stirred reactor models that do not account for TCI. Another widely used model is the flamelet approach [2] which relies on an assumption of fast chemistry that implies the formation of laminar flame structures embedded in a turbulent flow field. The coupling between turbulence and chemistry in flamelet-type models is usually achieved in a parametric way (e.g. via the scalar dissipation rate in non-premixed combustion), which means that there is no direct interaction between chemistry, molecular transport and turbulence. Existing regime- and mode- independent combustion models include transported PDF models with structure-based mixing models [3] and low-dimensional stochastic models such as LES-LEM, in which the linear eddy model of Kerstein [4] is used as a sub-grid model in a large-eddy simulation (LES) [5,6,7,8]. In LES-LEM a one-dimensional representation of the three-dimensional turbulent combustion process is solved in each LES cell by resolving all spatial and temporal scales on the one-dimensional domain, as done in direct numerical simulations as well. To overcome the high computational costs of LES-LEM while retaining some of its advantages, the authors recently proposed a new regime- and mode- independent combustion model called RILEM [1]. The RILEM approach solves only one representative linear-eddy model instantiation in the computational domain. The goal was to create a modeling approach that retains the key advantages of a full LES-LEM, namely regime and mode independence, at acceptable computational costs.

In the current study RILEM is used to simulate a sector-mesh engine simulation. The results are compared with the so called 'spray-B', an engine experiment performed at the Sandia National Laboratories within the Engine Combustion Network (ECN) [9]. Liquid and vapour penetration, ignition delay times, flame lift-off, heat release rates and pressure development computed with RILEM are compared to the experiments with different initial ambient temperatures at top dead center (TDC) of 800, 900 and 1000K. An earlier study from Mahgbouli et al. [10] used the same engine as presented here and applied two well established combustion models, namely the multiple representative interactive flamelet model (mRIF) and a well-stirred reactor model and compared the results. The study pointed out, that the mRIF model shows better agreement concerning flame lift-off data compared to the experiment than the well stirred approach. Ignition delay times were better predicted by the well stirred approach than by the mRIF model.

EXPERIMENTAL SETUP

Optical Engine and Diagnostic setup

The engine experiments used in this paper were carried out with an optical heavy duty 2.34 l diesel engine. Details concerning the engine appear in table 1. The injector used in this engine is the ECN Spray B #211199 three-hole injector. Details are shown in table 2. Fig 1 presents an outline how a part the optical measurements were performed. The setup shown in fig. 1 was used to measure the vapor penetration length. In addition to the presented equipment a Phantom v611 high-speed color camera and a beam splitter (R310 diachromic @45 deg) together with a second intensified monochrome Phantom 7.1 fitted with a bandpass filter of width 10 nm centered at 310 nm are used. The first of the described diagnostics is to get the liquid penetration length, the second is for determining the ignition delay and the lift-off length. More details on the conditions of the experiment can be found in [11].

Table 1: Sandia optical engine specifications [CITE]

Intake valves	2
Exhaust valves	1
Swirl ratio	0.5
Bore x Stroke	13.97 x 15.24 [cm]
Bowl width x depth	9.78 x 1.55 [cm]
Displacement	2.34 [L]
Compression ratio	11.22:1*
Connection rod length	30.48 [cm]

* TDC conditions typical of 16:1 CR are met by increasing the intake pressure and temperatures relative to ambient.

Table 2: Details of Sandia spray B injector: Orifice 3 was of interest in spray B experiments. Bottom: Orientation of orifices.

Inj. type	#211199 Bosch Spray B
Hole sizes: 1, 2, 3	90.9 µm, 91.7 µm, 90.9 µm
Nominal included angle	145 deg
Nozzle shaping	Smoothed
Discharge coefficient	$C_d = 0.86$
Hole angular position	1: 36.4, 2:-62.3, 3:180 deg

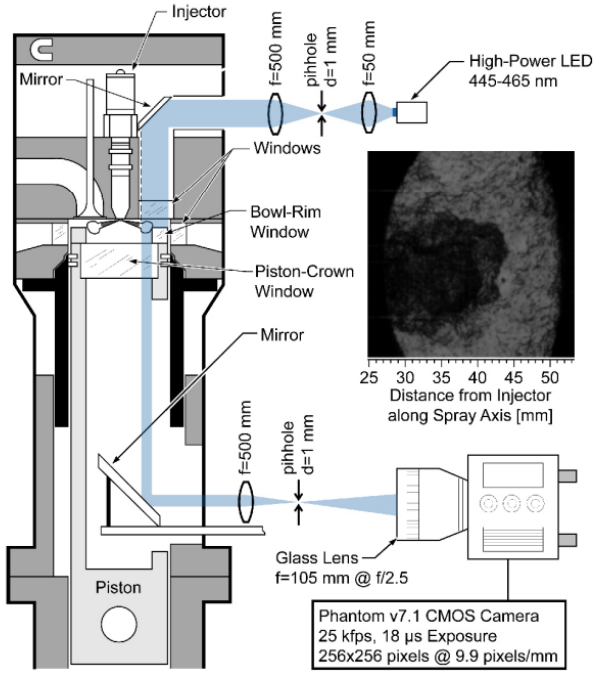

Figure 1: Schematic of extended-piston optical imaging schematic and Schlieren setup. Example of penetration depth at 364 CAD at ambient conditions of spray B basis case

Operating conditions

Several parameters of the Spray B experiments were changed. For each condition 30 to 90 injections are performed and the results presented are ensemble averaged. The full range of parameters are presented in [11]. The timing, duration and profile of the injection process were kept identical, but ambient gas and rail pressure conditions are changed. Cases are named after the targeted TDC condition of the variated parameter. Spray B is the basis with the in-Cylinder conditions 900K, 15% O2, 22.8 kg/m^3 and an injection pressure of 1500 bar. Two variations of the temperature, 800 and 1000K at TDC were performed by changing intake charge heating. 15.2 kg/m^3 were achieved by reducing the intake plenum mass-flow (pressure). The focus in this paper is on the cases were the temperature was changed. The case with a lower density was used in a non-reacting condition in order to obtain a reasonable spray setup for the simulations.

Liquid length and vapor penetration

Diffused back illumination (DBI) [12] is the techniques that ECN recommends to measure the liquid length. It has the advantage of self-calibration what makes it easy to compare between different facilities. However, in the optical heavy duty presented here the DBI setup is not suited. Instead, classical Mie scattering is used for the measurement. Intensity profiles along the spray axis for the 3 sprays are collected and the threshold is set to 3% of the maximum value, as suggested in [13]. The collected images give projected distances that must be converted into distances along the spray axis afterwards. A phantom v611 complementary metal oxide semiconductor camera (CMOS) at 67.1 kHz onto the red channel is used to get the images. The field of view is 40x40 mm^2 at an image size of 128x128 pixels (2.8pix/mm).

The vapor penetration is determined under non-reacting conditions by looking at Schlieren images of one penetrating diesel spray. To obtain measurements a collimated beam is directed through the engines upper viewport as can be seen in Fig.2. 1 image each 0.29 CAD at 1200 revolutions per minute (RPM) is generated by setting up a Phantom v7.1 CMOS camera at a frame rate of 25 kHz and an exposure duration of 40 micros. The results of 30 injections are ensemble averaged to get the vapor penetration. The field of view is 26x26 mm^2 at an image size of 256x256 pixels (9.9 pixels/mm). Optical access to the spray chamber is possible only between 26 and 50 mm, that is the reason why the technique proposed in [14] is not applicable. Here, the furthest point of the spray away from the nozzle is defined as the vapor penetration depth. Fig. 2 shows an example of a processed Schlieren image, where the blue line highlights the border of the spray and the red dot presents the place furthest away from the nozzle. The reported vapor penetration length in the results section is lengthened to compensate the spray angle of 14deg., which was specified for the spray B.

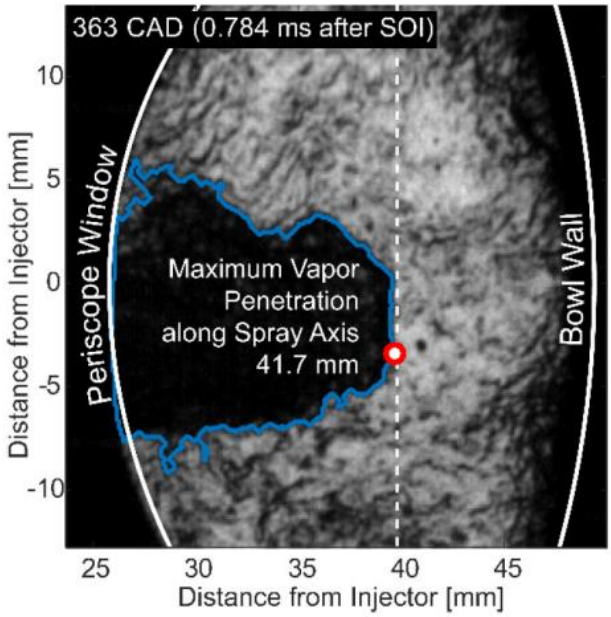

Figure 2: A processed schlieren image in non-reacting conditions for an ambient density of 15.2 kg/m^3. The frontier of the spray is indicated by the blue line, while the red dot presents the point of maximum vapour penetration.

Start of combustion, heat release and lift-off length

Simultaneously with the acquisition of the optical data, the cylinder pressure is digitized at every 0.25 CAD. Apparent heat release rates (AHRR) are calculated from filtered pressure data applying an air-standard first-law analysis [15]. A Fourier series low-pass filter with a Gaussian roll-off function having a transmission of 100% from 0 to 800 Hz and dropping to 1% at 3360 Hz. These frequencies were filtered out in order to remove acoustic noise in the cylinder pressure data, but keeping the characteristics of the AHRR. The start of combustion (SOC), advisable by the first positive AHRR, is typically moved forward from that for the unfiltered data up to 70 micros, depending on AHRR arising during the premixed portion after SOC. Supplementary the peak in the premixed burn tip is reduced and broadened, both by a factor of 2, ensuring the energy release during the premixed burn (integral of AHRR) to be virtually unchanged by this filtering technique.

The OH* chemiluminescence images are handled following the approach discussed in [16, 17]. The spray axis and two lines left and right of the axis are defined, forming the spray angle (± 5 deg). The lift-off is an average of the lift-offs on both lines left and right of the spray axis. Images are gained at 7.2 kHz using a monochrome Phantom v7.1 CMOS camera. The viewfield is 60x60 mm^2 at an image size of 512x512 pixels (8.5 pixels/mm).

COMPUTATIONAL SETUP

Numerical Framework

The CFD simulations were carried out using the open source code OpenFOAM [18]. The RILEM was implemented into OpenFOAM 2.2.x. The spray simulation are based on the Lib-ICE, a set of applications and solvers for internal combustion engines implemented by the ICE Group of Politecnico di Milano. RANS simulations are conducted for a full cycle (IVC to EVO) for the Sandia 'spray-B'. The standard k-ε model is used to model the turbulence with a modified constant $C_{\varepsilon 1}$ as suggested in the ECN workshop for n-dodecane sprays [19]. The Huh-Chang wall function models the heat transfer through the wall boundary layer [20]. An Eulerian-Lagrangian approach is used to model the spray break-up. The spray itself is represented by computational parcels, which represent droplets with identical properties. Here, the introduced parcels are of the same size as the nozzle diameter. The spray sub-models used in this work can be found in [21]. The KHRT model is used to model the droplet break up. Raleigh-Taylor break-up is only permitted after a certain distance from the nozzle, otherwise unphysical small droplets are formed. Droplet evaporation is computed following the D^2 law and the Spalding mass number, while heat transfer between liquid and gas phases is modeled using the standard Ranz-Marshall correlation. The numerical grid was generated with an automatic mesh generation tool implemented in the Lib-ICE code. It creates spray-oriented and fully hexahedral grids [22] as can be seen in fig. 3.

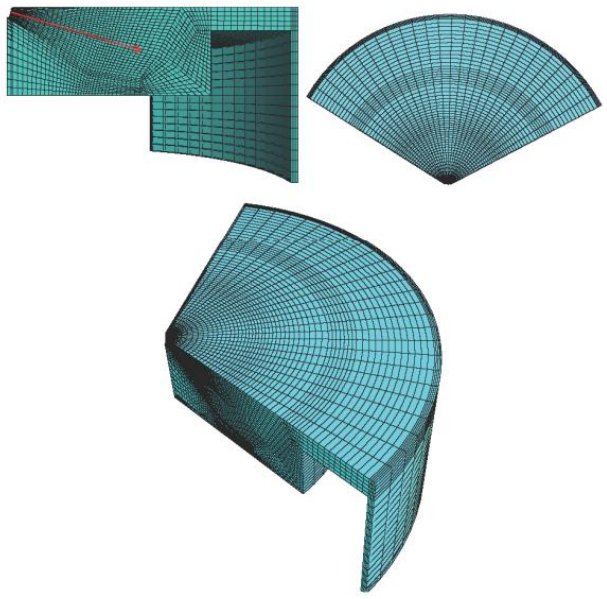

Figure 3: Numerical grid

Combustion modeling

Linear eddy model

The Linear-Eddy Model was proposed by Kerstein [23] as a scalar mixing model for non-reacting flows and subsequently extended to describe reactive flows [26]. It has been discussed at length in the literature [23, 24, 25, 26] and is, therefore, only briefly outlined here. The LEM describes turbulent reactive flows in terms of two concurrent processes representing the effects of dilatation-induced advection, molecular diffusion, chemical reactions, and turbulent transport. The first process is time advancement of the reactive zero-Mach-number equations in a one-dimensional domain [27, 28] resolving all spatial and temporal scales. The second process, turbulent transport, is implemented as a stochastic sequence of statistically independent eddy events. In the study presented here a spherical formulation of the LEM model has been applied that enables consistent representation of fuel distributions and fuel-air ratios compared to the full 3d geometry.

RILEM

On the CFD side the standard set of equations for global mass, momentum, and enthalpy and a standard Lagrangian spray model including single-component fuel evaporation are solved. Turbulence is modeled with the standard κ-ε (turbulent kinetic energy-turbulent kinetic dissipation). To characterize turbulent fuel-air mixing, additional transport equations for the mixture fraction $\tilde{Z}$ and the variance of the mixture fraction $\widetilde{Z''^2}$ are solved:

$$\frac{\partial(\bar{\rho}\tilde{Z})}{\partial t} + \nabla\cdot\left(\bar{\rho}\tilde{u}\tilde{Z}\right) = \nabla\cdot\left[\frac{\mu_t}{Sc_t}\nabla\tilde{Z}\right] + \dot{S}_{evap}\,, \qquad (1)$$

$$\frac{\partial(\bar{\rho}\widetilde{Z''^2})}{\partial t} + \nabla\cdot\left(\bar{\rho}\tilde{u}\widetilde{Z''^2}\right) = \nabla\cdot\left[\frac{\mu_t}{Sc_t}\nabla\widetilde{Z''^2}\right] + 2\frac{\mu_t}{Sc_t}(\nabla Z)^2 - \tilde{\chi}, \qquad (2)$$

where $\dot{S}_{evap}$, μ_t, and Sc_t are the source term due to evaporation, the turbulent viscosity, and the turbulent Schmidt number (which takes a constant value of 0.7), respectively.

The scalar dissipation rate $\tilde{\chi}$ is modeled as:

$$\tilde{\chi} = c_\chi \frac{\varepsilon}{k}\ \widetilde{Z''^2} \qquad (3)$$

with model constant $c_\chi = 2$.

The energy budget is solved in form of an equation for the total enthalpy $\tilde{h}$:

$$\frac{\partial\bar{\rho}\tilde{h}}{\partial t} + \nabla\cdot\left(\bar{\rho}\tilde{u}\tilde{h}\right) = \frac{d\tilde{p}}{dt} - \nabla\cdot j + \dot{q}_{evap}, \qquad (4)$$

where j is the heat flux vector and $\dot{q}_{evap}$ is the enthalpy source due to droplet evaporation, which comes from the spray model. Viscous heating has been neglected here, which is a reasonable assumption for low Mach-number flows.

Once the enthalpy equation is solved, the temperature can be calculated via the caloric equation of state:

$$\tilde{h} = \sum_{s=1}^{N} \tilde{Y}_s\, h_s(\tilde{T})\ , \qquad (5)$$

where h_S denotes the mass-specific enthalpy of species s including the heat of formation and the temperature-dependent sensible enthalpy. The Favre-averaged species mass fractions $\tilde{Y}_S$ in each cell of the computational domain are obtained by integrating LEM mass fraction values mapped onto mixture fraction space using a presumed β-PDF for the mixture fraction:

$$\tilde{Y}_S = \int_0^1 P\left(Z,\tilde{Z},\widetilde{Z''^2}\right) Y_S^{LEM}(Z)\,dZ\,. \qquad (6)$$

Here, $Y_s^{LEM}(Z)$ denotes the mass fraction of species *s* obtained from the representative LEM, which has been mapped from the physical space of the LEM domain onto mixture fraction space. This mapping features an important distinction from flamelet models. Due to the stochastic nature of the LEM, an arbitrary number of different thermodynamic states are possible for a fixed mixture fraction value. This variability of states for a given mixture fraction reflects the inherent variability of scalar dissipation rates in the LEM. The PDF of the scalar dissipation rate is an outcome of the solution, whereas in sharp contrast it is an input parameter for flamelet models.

Figure 4 presents the basic structure of the RILEM code. CFD and representative LEM solutions are time-advanced in an alternating manner. First the fluid dynamics are calculated for one time step on the CFD side, then the LEM is supplied with updated variables for the pressure change, characteristic turbulent length and velocity scales, and information about the evaporated fuel mass. The fuel is inserted in the middle of the (spherical) LEM domain [29].

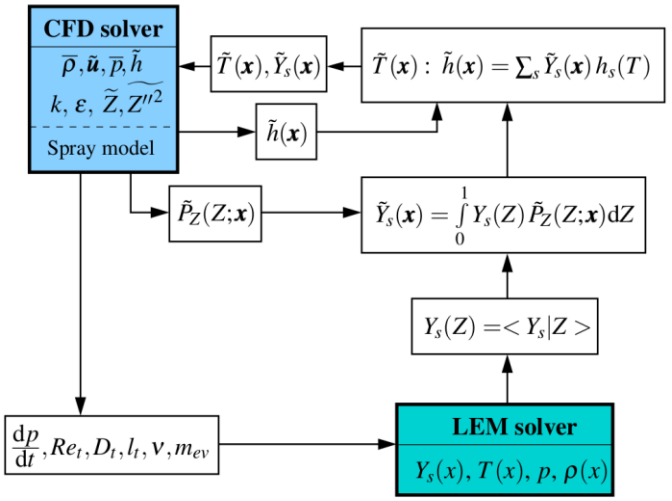

Figure 4: The RILEM code structure

Definition of Quantities

In order to obtain initial conditions for the start of combustion simulations, motored conditions without injection were carried out. Good agreement for pressure and temperature at TDC are a prerequisite for successful simulations. The comparison of experimental data and numerical results is based on the following definitions:

- **Liquid length**: Maximum distance from the nozzle to a Lagrangian parcel in which 95% of the mass is in liquid form.
- **Vapour penetration**: The distance between the nozzle and the cell with a mixture fraction larger than 0.001

furthest away from the nozzle is considered as the vapor penetration length.

- **Ignition delay**: AHRR of simulations are calculated by applying thermodynamic first law analysis analogous to the experiments. Similar approaches for filtering the AHRR were applied. The crank angle with a maximum rise of the AHRR is the point where the mixture is considered as ignited. There are different ways to define ignition delay. Other studies used the maximum rise of the Favre averaged temperature [30] or a temperature rise of 400K at the point of ignition [22].

- **Flame lift-off length**: The flame lift-off is defined as 14% of the maximum OH concentration at that operating condition [31]. This is the definition that is used within the ECN.

Results and Discussion

The quantities for the non-reacting conditions including liquid length and vapor penetration depth are presented first, followed by the quantities that were measured and computed under reacting conditions, namely AHRR, pressure traces, ignition delay and flame lift-off length.

Non reacting conditions

A good description of the spray process is essential for accurate description of ignition and combustion processes. Thus, results of the simulation of a non-burning spray were compared to data acquired under corresponding conditions at the Sandia National Laboratories. Figure 5 shows the liquid length for the different cases for the Experiments and the simulations. All cases exhibit good agreement between the experiments and the simulations, although the simulations slightly overpredict the liquid penetration for all conditions. Unfortunately, the authors only had access to vapor penetration data for the lower density case. The vapor penetration was evaluated for that lower density case.

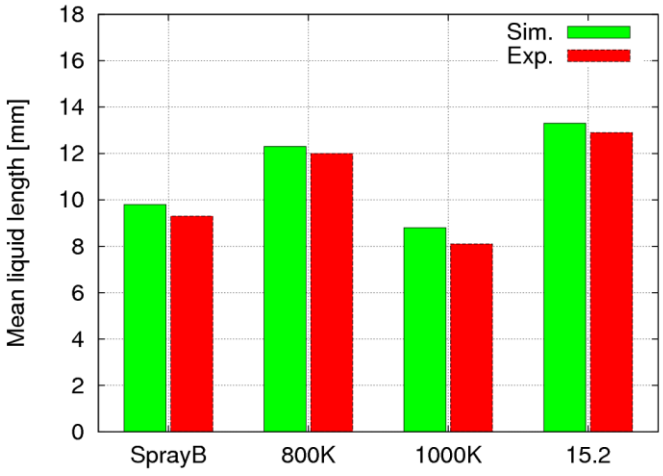

Figure 5: Simulated and experimentally determined liquid penetration depth for all cases

Figure 6 compares the experimental and simulated temporal evolution of the vapour penetration length for the lower density case. Similar to the liquid length the vapor penetration depth is captured well by the numerical simulations.

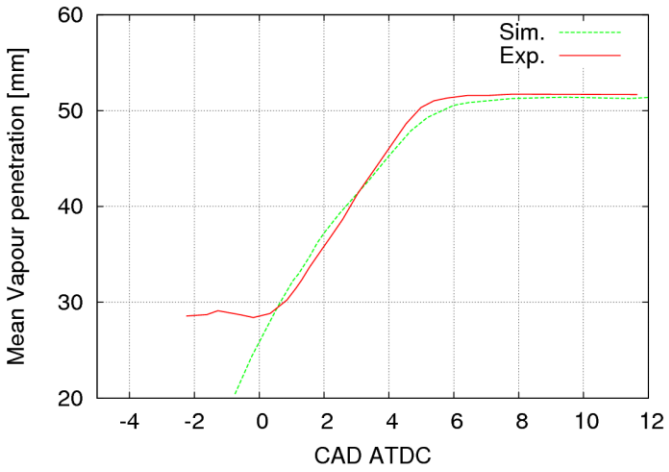

Figure 6: Simulated and experimentally determined vapor penetration depth for case x (7.5 % O_2, 900K, 15.2 kg/m^2)

Reacting conditions

Ignition delay time

Figure 7 shows the ignition delay times for the temperature variations. The ignition delay times are underestimated for all cases. The reason is the chemical mechanism used in this study. At the ECN workshop [31] it was shown that the ignition delay time is mainly governed by the chemical mechanism and not so much by the individual combustion model. Different models were used with the same chemical mechanism, which produced similar results for ECNs so called spray-A, a spray combustion bomb fueled with n-dodecane. It was reported that the reason for the wrong ignition delay predictions of the chemical mechanism is the lack of precise experimental ignition delay data in the high temperature region which leads to unprecise chemical mechanisms. New experimental data is needed that enables the development of more precise chemical mechanisms. The quantitative results for the ignition delay times in this study are in the same range as the ones reported at the ECN workshop [31] for the particular mechanism used in this study.

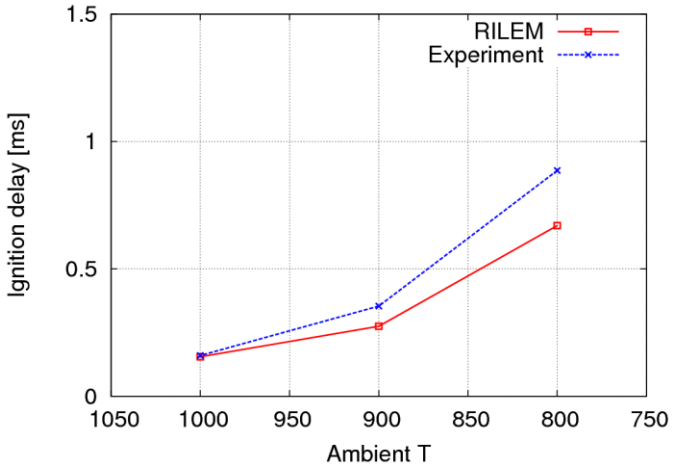

Figure 7: Ignition delay times for all cases

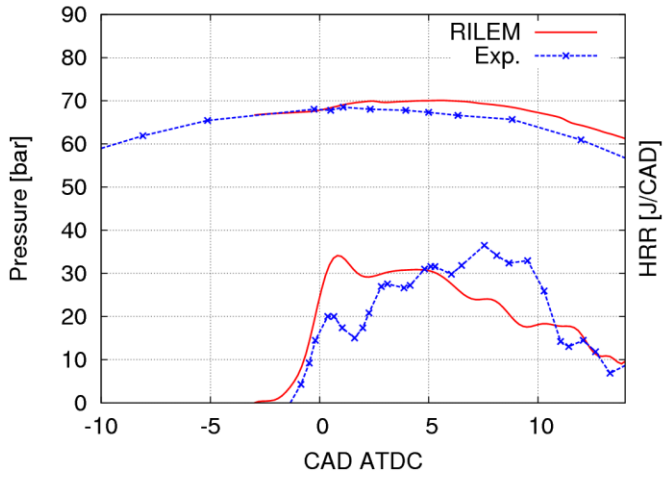

Figure 8: Cylinder pressure and AHRR computed with RILEM compared to experimental data for the 1000K case

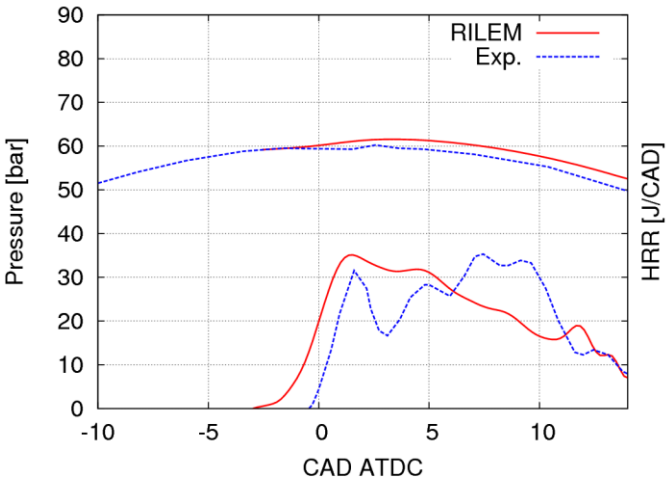

Figure 9: Cylinder pressure and AHRR computed with RILEM and experimental data for the 900K case

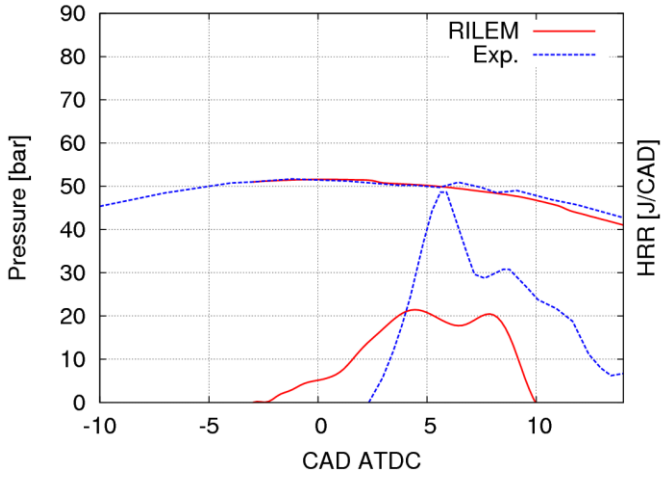

Figure 10: Cylinder pressure and AHRR computed with RILEM and experimental data for 800K case

Pressure and heat release rate

Figures 8-10 compare computed and experimental heat release rates for the three different temperature cases. The main effect of the temperature variation on the experimental results seems to be the amount of fuel which burns during the premixed combustion phase in the beginning of the combustion process. The highest premixed peak can be seen for the low temperature case where the mixture has the longest time to mix resulting in locally premixed conditions at the point of ignition. For 900K this peak can be still recognized but it almost vanishes for the 1000K case. The cylinder pressure is slightly over-predicted by RILEM compared to the experimental data for 900 and 1000K. Due to the earlier ignition (compared to the experiments) the heat release peaks earlier what causes a higher pressure in the beginning of the combustion phase. During the combustion period the pressure difference between the experimental data and the simulation stays constant. The heat release rate of RILEM shows a small peak in the beginning, similar to the experiments but with higher absolute values. The increase in the AHRR in the beginning is the same for the RILEM and the experiment. When combustion starts the AHRR is over-predicted by the RILEM, but after 5 CAD that changes into an under-prediction of the AHRR by the model. The integral under the curve is similar indicating that the same heat is released in the combustion chamber for the cases with 1000 and 900K. The RILEM shows overall acceptable results for 1000 and 900K. However, for 800K RILEM fails to predict the heat release rate. The strong pronounced premixed peak in the beginning seems not to be captured by the model. Instead the mixture ignites much earlier and does not reach the high levels of AHRR measured in the experiment. In addition the released heat in the combustion chamber is too low. The reason for this behavior has not been clarified yet but will be addressed in a further studies of the model.

Flame brush and lift-off lengths

In fig. 11 the lift-off lengths computed with the RILEM for the three different cases are shown. The predicted flame lift-off is shorter than the measured one. The reason is that RILEM as its state now just computes a mixing controlled flame lift-off. Once the LEM domain is ignited, this ignited solution is mapped back to the CFD domain to all cells. That is why it is not possible to fully describe the injection of fuel and its auto-ignition while it evolves inside the computational domain with a single RILEM as used here. Multiple RILEMs or decomposition of the single RILEM into domains with different mixing times are potential strategies to overcome the problem. They will be investigated in further studies. The OH-contours for the 1000K case computed with the RILEM and scaled to the maximum and the threshold of 14% of the maximum OH concentration at 6 CAD ATDC are presented in fig. 12. The predicted lift-off with RILEM is about 7 mm for the 1000 K case. The underestimation of the flame lift is the bigger the longer the chemical ignition delay is. For the 800K case the RILEM underestimates the lift-off by almost half of the measured length.

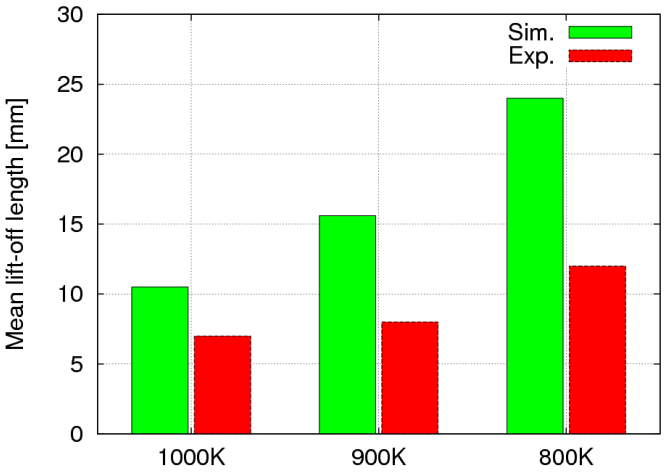

Figure 11: Cylinder pressure and AHRR computed with RILEM and experimental data for the 900K case

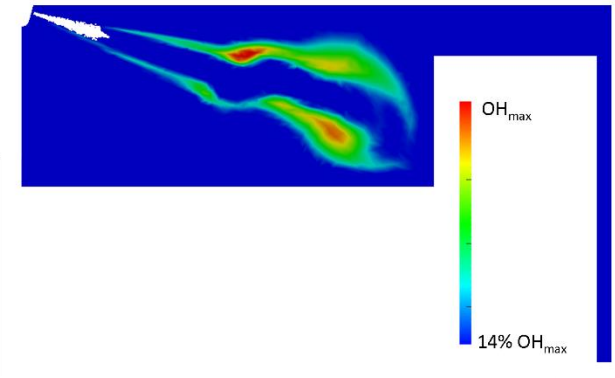

Figure 12: Spatial OH contour of the 1000K case computed by RILEM on a plane through the injection axis and normal to the cylinder wall. The white dots present the liquid fuel.

CONCLUSION

The aim of this paper was to apply RILEM, a recently developed combustion model, for the first time to diesel engine combustion. The presented results show that RILEM is able to predict an engine combustion case with some limitations. The representative LEM is solved concurrently with advancement of the CFD simulation and enables direct interaction between the flow solution on the CFD side and the combustion process carried out at all length and time scales on the one-dimensional domain of the LEM line.

In order to evaluate the performance of the model it was used to simulate a diesel engine combustion case, the so called 'spray-B', which was realized within the ECN. A large set of data over a broad range of parameters is available for this engine campaign. In this work, the focus was on three cases with varying TDC center temperatures. The liquid length, vapor penetration, in-cylinder pressure, AHRR, ignition delay time and flame lift-off of the model and experiments were compared. Liquid and vapor penetration comparisons were performed under non-reacting conditions. It turned out that the used models reproduced the spray reasonable well. Simulated ignition delay times were generally under-predicted, which is in line with the findings at the ECN workshop for the chemical mechanism used in this study. The AHRR were captured rather well, with some over-prediction of the AHRR during the start of combustion which leads to a slightly over-predicted pressure trace after combustion started. An exception is the low temperature case. Simulations fail to predict the AHRR. The flame lift-off is purely mixing controlled what leads to an under-prediction of the lift-off length compared to experiments, which was found to grow with increasing ignition delay time.

REFERENCES

1. Lackmann, T., Kerstein A. R., Oevermann, M., SAE Technical Paper Series, 2015.

2. Peters, N., Prog. Energy and Combust. Sci., 10, 319-339, 1984.
3. Meyer, D. W., and Jenny, P., Physics of Fluids, 18:035105, 2006.
4. Kerstein, A. R., Comb. Sci. Tech., 60:391-421, 1988.
5. El-Asrag, H., Menon, S., Combustion and Flame, 156:385-395,2009.
6. El-Asrag, H., Lu, T., Law, C. K., Menon, S., Combustion and Flame, 150:108-126, 2007.
7. Sen, B. A., Combustion and Flame, 157:62-74, 2010.
8. Sen, B. A., Menon, S., Combustion and Flame, 157:566-578, 2010.
9. Sandia Engine Combustion Network Database. http://www.ca.sandia.gov/ecn, 2015.
10. Maghbouli, A., Lucchini, T., D'Errico, Onorati, A. et al, SAE Technical Paper Series, 2016.
11. Eagle, W., Malbec, L., and Musculus, M., "Measurements of liquid length, vapor penetration, ignition delay, and flame lift-off length for the Engine Combustion Network `Spray∼B' in a 2.34L Optical Heavy-Duty Diesel Engine," SAE Technical Paper 2016-01-0743, 2016, doi:10.4271/2016-01-0743.
12. SANDIA Engine Combustion Network. sandia.gov/ecn/cvdata/ expdiag/liqlenspraya.php, 2015.
13. Siebers, D., "Scaling Liquid-Phase Fuel Penetration in Diesel Sprays Based on Mixing-Limited Vaporization," SAE Technical Paper 1999-01-0528, 1999, doi:10.4271/1999-01-0528.
14. Naber, J. and Siebers, D., "Effects of Gas Density and Vaporization on Penetration and Dispersion of Diesel Sprays," SAE Technical Paper 960034, 1996, doi:10.4271/960034.
15. Heywood J. B.. *Internal Combustion Engine Fundamentals*. McGraw-Hill, 1988.
16. Higgins, B. and Siebers, D., "Measurement of the Flame Lift-Off Location on DI Diesel Sprays Using OH Chemiluminescence," SAE Technical Paper 2001-01-0918, 2001, doi:10.4271/2001-01-0918.
17. Siebers, D. and Higgins, B., "Flame Lift-Off on Direct-Injection Diesel Sprays Under Quiescent Conditions," SAE Technical Paper 2001-01-0530, 2001, doi:10.4271/2001-01-0530.
18. Weller H.G., Tabor G., Jasak H., and Fureby C.. A Tensorial Approach to CFD using Object Orientated Techniques. *Computers in Physics*, Vol. 12(No. 6):620, 1998.
19. Bhattacharjee S. and Haworth D. C.. Simulations of transient n-heptane and n-dodecane spray flames under engine-relevant conditions using a transported PDF method. *Combustion and Flame*, 160(10):2083-2102, 2013.
20. Huh, K., Chang, I., and Martin, J., "A Comparison of Boundary Layer Treatments for Heat Transfer in IC Engines," SAE Technical Paper 900252, 1990, doi:10.4271/900252.
21. Maghbouli A., Lucchini T., D'Errico G., and Onorati A.. Effects of grid alignment on modeling the spray and mixing process in direct injection diesel engines under non-reacting operating conditions. *Applied Thermal Engineering*, 91:pp. 901-912, 2015.
22. Bhattacharjee S. and Haworth D. C.. Simulations of transient n-heptane and n-dodecane spray flames under engine-relevant conditions using a transported PDF method. *Combustion and Flame*, 160(10):2083-2102, 2013.
23. Kerstein, A. R., Combustion Science and Technology, 60:391-421, 1988.
24. Kerstein, A.R., Combustion and Flame, 75:397-413, 1989.
25. Kerstein, A.R., Journal of Fluid dynamics, 240:289-313, 1992.
26. Kerstein, A.R., Combustion Science and Technology, 81:75-96, 1992.
27. Oevermann, M., Schmidt, H., Kerstein, A. R., Combustion and Flame, 155:370-379, 2008.
28. Schrödinger, C., Paschereit, C. O., Oevermann, M., Combustion Science and Technology, 186:1392-1409, 2014.
29. Lackmann, T., Kerstein, A., Oevermann, M., European Combustion Meeting, Budapest, 2015.
30. Pei Y., Hawkes E. R., Kook S., Goldin G. M., and Lu T.. Modelling n-dodecane spray and combustion with the transported probability density function method. *Combustion and Flame* 162, no. 5, pages pp. 2006-2019, 2015.
31. Hawkes E.R.. Engine combustion network workshop two: Ignition and lift-off session, 2012.

CONTACT INFORMATION

Tim Lackmann
Division of Combustion
Department of Applied Mechanics
Chalmers University of Technology
SE-41296 Gothenburg, Sweden
tim.lackmann@chalmers.se

ACKNOWLEDGMENTS

The authors would like to thank Chalmers Combustion Engine Research Center (CERC) for financial support.